CRYSTALLINE SICO:IMPLICATION ON STRUCTURE AND THERMOCHEMISTRY OF TERNARY SILICON OXYCARBIDE CERAMICS

by

NELLI BODIFORD

Presented to the Faculty of the Graduate School of

The University of Texas at Arlington in Partial Fulfillment

of the Requirements

for the Degree of

MASTERS OF SCIENCE IN CHEMISTRY

THE UNIVERSITY OF TEXAS AT ARLINGTON

May 2013

ACKNOWLEDGEMENTS

This work would not have been possible without the guidance and help of several individuals who have greatly contributed and provided their help in the preparation and completion of this study.

My best gratitude goes to Dr. Peter Kroll, my supervisor and the associate professor at the University of Texas at Arlington, whose support and encouragement I will never forget. Dr. Kroll has provided a great deal of support and inspiration in the pursuit of this study and helped me hurdle all the obstacles throughout this research work.

I would like to thank my lab mates: Munuve Mwania, JP Nimmo and Atreyi Dasmahapatra for their stimulating discussions and for all the fun we had during the last three years.

At last, I would like to thank all my family for their incredible help and for giving me the moral and financial support I needed to proceed with my studies: Bill and Denise, my mom, and Miles.

March 29, 2013

ABSTRACT

CRYSTALLINE SICO:IMPLICATION ON STRUCTURE
AND THERMOCHEMISTRY OF TERNARY
SILICON OXYCARBIDE CERAMICS

Nelli Bodiford, M.S.

The University of Texas at Arlington, 2013

Supervising Professor: Peter Kroll

The need for innovative refractory materials – materials that can sustain extreme temperatures – has been constantly growing within the modern industries. Basic requirements for usage at ultra-high-temperatures have been considered such as high melting point, high structural strength, exceptional resistance to oxidation, zero or almost zero creep. Monolithic ceramics alone cannot provide these properties, therefore, composite materials are sought to fulfill the demand. For example, silicon nitride and silicon carbide based ceramics have long been leading contenders for structural use in gas turbine engines. In the course of this work we are investigating amorphous SiCO formed via polymer-to-ceramic route. Previously a considerable amount of work has been done on structures of stoichiometric amorphous SiCO and a “perfect” random network was obtained (experimentally as well as supported by computational work) up to the phase content of 33 mol-% SiC. By “perfect” one assumes to have four fold coordinated Si atoms bonded to C

and O; C atoms bond to Si atoms only and O is two fold connected to Si. Beyond 33 mol-% SiC within SiCO phase the structural imperfections and defects start to develop.

Aside from the stoichiometric form of SiCO, the polymer-to-ceramic route allows for the incorporation of high molar amounts of carbon to create SiCO ceramic with excess carbon. The incorporation of carbon into silica glass improves high-temperature mechanical properties and increases resistance to crystallization of the amorphous material. The amount of 'free carbon' can be controlled through the choice of precursors used during synthesis.

There were no ternary crystalline phases of SiCO observed. However, in systems such as MgO-SiO_2, Na_2O-Al_2O_3-SiO_2 there are ternary crystalline compounds ($MgSiO_3$, Mg_2SiO_4, $NaAlSiO_4$, $NaAlSi_3O_8$) that are of a greater energetic stability than glasses of the same composition. What makes the SiCO system different?

In the approach proposed in this work for studying the SiCO system we work with crystalline models. These are well-ordered structures that approximate essential details of a disordered phase. The crystalline models are generated by using recently introduced structure search algorithms: AIRSS (*Ab Initio* Random Structure Prediction Search) and USPEX (Universal structure predictor: Evolutionary Xtallography). Then the models are further optimized in a standard ab-initio total-energy and molecular dynamics program VASP (Vienna Ab-initio Simulation Package) using pseudopotentials, plane waves, and the generalized gradient approximation (GGA). Structures of the targeted compositions start with 10 mol-% of SiC within SiCO up to 66 mol-%. In addition to stoichiometric models, we also analyzed structures with "free" carbon. The excess energy was calculated from the difference between the energy of the model and the energy of a combination of phase assembly composed of β-SiC, q-SiO_2 and graphite.

As the result, this work presents SiCO crystalline models, their microstructure, crystallographic description of each structure, energetic stability compared to amorphous

models as well as the phase diagrams including Gibbs energy calculations to estimate thermodynamic stability.

TABLE OF CONTENTS

LIST OF ILLUSTRATIONS

Figure
Page

LIST OF TABLES

CHAPTER 1

INTRODUCTION: SIGNIFICANCE OF PDC MATERIALS WITH THE EMPHASIS ON SICO SYSTEM

1.1 Introduction to polymer-derived ceramics: SiCO

Polymer-derived ceramics (PDCs) represent a class of materials that are processed using preceramic polymers. This polymer to ceramic transformation route presents several major advantages over the traditional method for preparing ceramics. The traditional way of preparing ceramics involves powder technology, which in turn requires the presence of sintering additives that very often can have a negative impact on the microstructure and the fracture strength of the material. Moreover, the traditional method imposes additional constraints on the form and shape of ceramics. PDCs on the other hand, produced starting from the preceramic polymers require no additives and can be formed into a variety of shapes and coatings including fibers, layers, or composite materials. In addition, the relatively low synthesis temperature for making PDCs, 1100-1300^{o}C allow for a lower energy consumption compared to powder technology [1]. Thus, PDCs are additive-free ceramic materials with remarkable structural and functional properties, among which are high mechanical strength, resistance to oxidation and corrosion, and high temperature stability [2, 3].

Several classes of ceramics can be synthesized via a polymer-to-ceramic approach. Well-known classes of PDCs are in the binary systems SiC, BN, Si_3N_4 and AlN followed by ternary systems SiCO and SiCN as well as the quaternary systems SiBCO, SiBCN, SiCNO [4]. This class of materials shows exceptional properties that make them suitable for multiple applications that include high-temperature-resistant materials, hard materials, functional materials in electrical engineering as well as in micro and nanoelectronics [5].

In this work the focus is on the family of ternary silicon oxycarbide PDC's. SiCO ceramics can be synthesized with different compositions and the availability of cheap precursors makes this material appealing. The process of formation of PDC's consists of three major steps: 1) synthesis of preceramic polymers; 2) polymer cross-linking; 3) ceramization process or commonly referred to as pyrolysis of the cross-linked material [6]. This transformation route results in a complex microstructure evolution of the end ceramics product. Silicon oxycarbide material can be synthesized in three forms: stoichiometric SiCO, C-rich SiCO and Si-rich SiCO. In this work, we study stoichiometric SiCO and SiCO:C_{free} , where C_{free} is a so called "free carbon" phase. Figure 1.1 shows the composition diagram with the regions for stoichiometric SiCO and carbon-rich SiCO.

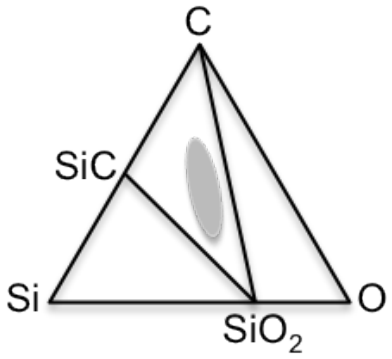

Figure 1.1. Composition diagram for SiCO. Stoichiometric SiCO lies on a tie-line between SiC and SiO_2. The grey region approximately marks the location for the carbon-rich SiCO.

Stoichiometric SiCO obtained via pyrolysis at 1000^0C is characterized as a fully amorphous structure by x-ray diffraction and electron microscopy [7]. Nuclear magnetic resonance (NMR) analysis shows SiCO glasses primarily as a network of $SiC_{4-x}O_x$ tetrahedra, which are randomly distributed in the material [8]. High-resolution transmission electron microscopy (HRTEM) analysis of stoichiometric SiCO annealed at 1200^0C shows regions with β-SiC crystallites 2-4 nm in size [7]. Thus the material is described as SiC crystallites

embedded in SiO_2 matrix, which leads to the formation of SiC-SiO_2 interfaces. These interfaces represent extended SiCO interphases.

The controlled thermal transformation at 1500^{o}C of polymers to ceramic yields a predominantly amorphous SiCO as a mixture of amorphous SiO_2 and crystalline SiC [7, 9]. This resistance to crystallization is considered one of the most remarkable properties of SiCO material. At around 1300°C small clusters of crystalline SiC start to precipitate slowly [7], while the silica portion of the ceramic remains amorphous up to 1500^{0}C. Note that pure amorphous silica crystallizes at around 1200°C into cristobalite-SiO_2 [10]. Regions of ordered graphite in the SiCO ceramic become visible at 1200°C and grow with increasing temperature. Raman analysis after heat treatment at 1400^{0}C shows the presence of graphitic carbon phase and energy filtered transmission electron microscopy (EFTEM) revealed some large turbostratic carbon domains (15-20 nm) at 1400-1450^{0}C [11, 12]. While the realm of amorphous SiCO ceramics is plentiful, no crystalline ternary SiCO phase has been observed so far.

Results from calorimetric studies of amorphous SiCO ceramics indicate substantial exothermic heats of formation from crystalline silica, silicon carbide, and graphite [13]. For the low-carbon sample a value of ΔH_{SiCO} is -17.8 +/- 7 kJ/mol and for the high-carbon sample the value of ΔH_{SiCO} is -128.2 +/- 7.1 kJ/mol. These results are puzzling, since they identify some amorphous SiCO ceramics – synthesized via a non-equilibrium route such as the polymer-to-ceramic conversion – to be thermodynamically stable. Contrary to these findings, previous modeling and simulation studies had shown that the enthalpy of formation of stoichiometric SiCO glass increases as the SiC content increases [14, 15]. Additional computational studies addressed the embedding of aromatic carbon and graphene in SiCO and focused on possible interface structures that may appear in SiCO containing free carbon [16]. However, the results pointed towards a significant energy penalty associated with the incorporation of C in SiCO, yielding to high enthalpies of formation.

To address the puzzles set by reported exothermic heats of formation, lack of ternary crystalline structures, and endothermic energies of formation found in computations, we set out to investigate crystalline SiCO and study structure and energy of crystalline models. The total energy and atomic structures of these models are calculated within density functional theory (DFT) [17]. The application of such calculations as predictive tools in solid-state chemistry has been demonstrated in numerous cases. Successful examples of the related systems are found within prediction and validation of SiO_2 polymorphs [18] and polytypes of SiC [19].

The underlying rationale of our endeavor is that among crystalline structures we will find trends of local and extended coordination and bonding that govern low-energy states, eventually finding one or more structures with energy lower than previously reported models of amorphous SiCO. In this work we present crystalline approximants of stoichiometric SiCO that can be composed of SiC and SiO_2, thus $SiC_xO_{(2-2x)} = xSiC + (1-x)SiO_2$ and compare their energy to that of amorphous models. The composition of interest ranges from 10 %mol SiC to ~66 % mol SiC content within SiCO system. Previously it was reported that the perfect random network is retained up to a phase content of 33 mol% SiC beyond this point thus with a higher content of SiC structural defects begin to develop [15]. In addition, models with an excess carbon within SiCO are presented that are composed of SiC, SiO_2 and graphite: $SiC_xO_{(2x-2)}C_y$. The goal is, on one side, to find well-ordered lowest energy structures for a given composition of SiCO. On the other side, we also gather understanding of the thermochemistry, in particular of the strong stabilization of the amorphous state of ternary SiCO. Since binary phases β-SiC and SiO_2 (quartz) are the end members of the SiO_2-SiC tie line, we include them in the study of ternary crystalline SiCO. The results of obtained energy values for the structures of different compositions and their implications on the feasibility of ternary crystalline SiCO are outlined further in this work.

CHAPTER 2

MODELING APPROACHES OF CRYSTALLINE SICO

2.1 Introduction to modeling

The structural characterization of amorphous SiCO has been addressed with the overviews in the articles of Brequel [20] and Corriu [8] along with the computational-modeling contributions of Kroll [14-16]. Key structural features include the amorphous nature of the material, presence of $SiC_xO_{(4-x)}$ -tetrahedra, the presence of a "free" carbon phase and the persistence of 1-5 nm size domains within the material [21]. The results of the previous computational work reported a "perfect" random network for the material, with up to 33-mol% of SiC in the glass. This "perfectness" of the network refers to the fact that all Si atoms are four-fold connected, as are the carbon atoms. While carbon bonds to Si only, Si bonds to both C and O. O is two-fold coordinated by Si [15].

Recent calorimetric measurements reported a negative enthalpy of formation for some amorphous SiCO and attributed it to the structural nature of the material [22]. Varga *et al* proposed that a nanodomain environment rich with grain boundaries led to interfacial energies, which in turn were likely to be a source of the negative enthalpy of the SiCO ceramics. They also suggested that the mixed tetrahedra of silicon $SiC_xO_{(4-x)}$ could be a macroscopic crystalline phase holding the SiCO structure together and contributing to the thermal stability of the material. There was still no specific explanation proposed at a microscopic level for the negative enthalpy of formation of this material, though Figure 2.1 shows the proposed arrangement of nanodomains within SiCO [21].

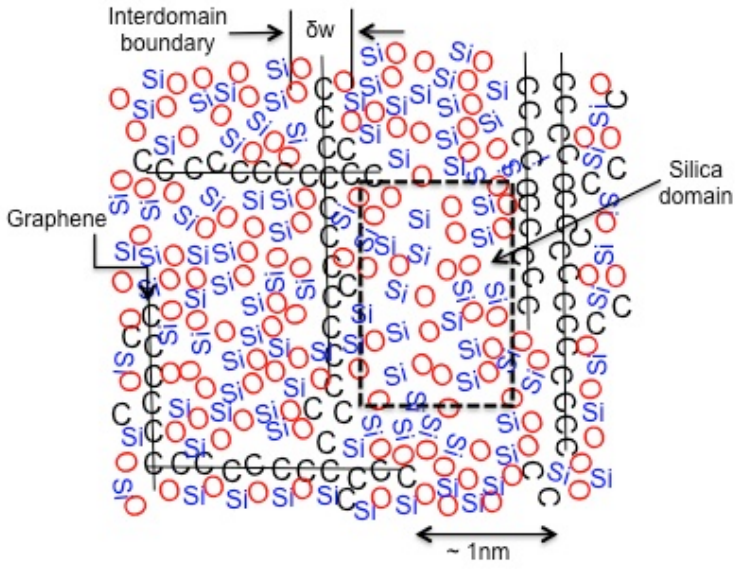

Figure 2.1 Nanodomain arrangement of SiCO. Graphene layers form an interface with silica and with mixed tetrahedra of silicon, where the interdomain boundaries appear [21].

In the following work, modeling and computational methods are employed to obtain results with respect to structural trends and thermochemistry of SiCO material. A large database of crystalline SiCO models is generated that includes stoichiometric SiCO and carbon-rich SiCO models. The goal is to generate a manifold of possible bonding environments using short-range crystalline models for the amorphous SiCO, to find indications for the negative enthalpy of formation and, not at last, to state whether there is a stable ternary phase of SiCO. The results also address the bonding interface between the “free” carbon and the glassy phase. Overall, this work contributes to the structural and energy aspects of amorphous SiCO ceramics.

2.2 Implementation of AIRSS and USPEX: structure database formation

The computational approach implemented in this work consists of two steps. First, SiCO crystal structures are generated using *Ab Initio* Random Structure Search algorithm (AIRSS) [23]. AIRSS is interfaced with Vienna *Ab Initio* Simulation Package (VASP) code for quantum mechanical calculations [24-27]. During the first step, crystal structures are randomly generated with a rough energy assessment. Following the search, all duplicate structures are excluded and the remaining unique structures are ranked by enthalpy. In the second step, the

best-chosen models are optimized again to ensure the appropriate convergence of energies. In this chapter the detailed overview is given on how the search algorithms along with the quantum codes are implemented to predict crystalline structures and their thermodynamic stability.

To generate and evaluate periodic structures of SiCO we used AIRSS [23]. The approach is simple, as it requires only few parameters. A set of unit cell lengths (a, b, c) and angles (α, β, γ) can be chosen. An appropriate volume is determined from known structures composed of the same atoms by adding up atomic volumes. AIRSS works by placing atoms randomly into a unit cell with random lattice parameters (under periodic boundary conditions), and thereafter optimizing atomic positions and the cell geometry. The number of atoms placed into the unit cell depends on the composition and the number of formula units. In our search for SiCO structures we worked with up to 80 atoms in the unit cell. While structures with only a few atoms (e.g. one formula unit) are quickly computed, larger structures take longer due to the computational costs during optimization, but did in some cases turned out to be more favorable. For instance, our lowest energy structure of Si_2CO_2 contains 8 formula units, thus 40 atoms in the unit cell.

Complementary to AIRSS we used the USPEX-code (Universal Structure Predictor: Evolutionary Xtallography) [28]. Evolutionary algorithms are potentially self-improving. In other words, if good structures are found they can be used to generate new structures, which retain favorable motifs and may yield lower energy. This approach typically converges rapidly to promising regions of the phase space where structures competing for the lowest energy structure can be found. In USPEX calculations we considered systems with up to 20 atoms in the primitive unit cell.

USPEX features three variation operators: heredity, mutation and permutation that are implemented to ensure the best structure generation. These operators are described in detail in Ref [28] sec. 2.2. Candidates (structures) for the initial population are either randomly generated (similar process to AIRSS) or can be provided by the user. A user needs to provide lattice

parameters and atomic coordinates: there are six lattice parameters, three angles (α, β, γ) and the length of three vectors. The probability of an individual structure being chosen depends on its fitness value. The fitness values are the negative of the *ab initio* energy that is used for the comparison between structures. During the search, the worst structures are removed from the pool and the rest of the structures remain and get locally optimized. The calculations of energies of the remaining structures continue, during which once again the worst ones are discarded and the best structures move on to the next level. A user can control the number of new structures produced along with the number of operations that need to be performed.

2.3 Hand-crafted models of SiCO structures

In addition to the structures generated with AIRSS and USPEX, we constructed a few handcrafted models of SiCO. On one hand, we wanted to compare them to the structures generated by AIRSS and USPEX; on the other hand, to create structures with over 200 atoms in a unit cell that are impractical to generate with search algorithms. Furthermore, we were interested in creating other possible bonding scenarios such as three-fold coordinated carbon or three-fold coordinated silicon atoms. For instance, we looked at high dilution of SiC in SiO_2 using a 3x3x3 super cell of α-quartz SiO_2 ($Si_{81}O_{162}$) replacing one SiO_4^{4-} unit by C^{4-}. As a result, the composition of the final structure was $Si_{80}CO_{158}$:$(SiC)_1(SiO_2)_{79}$. Likewise, in β-crystobalite SiO_2, SiO_4^{4-} unit was replaced with C^{4-}, thus Si_8O_{16} becomes Si_7CO_{12}: $(SiC)_1(SiO_2)_6$. After DFT optimization, the handcrafted model exhibited tri-planar carbon, four-fold coordinated Si and linear O. This model can be found in Figure 2.3.

A model containing three-fold coordinated carbon $C^{\{3\}}$ has been created from a structure of filled β-quartz SiO_2, $LiAlO_2$. In the structure of $LiAlO_2$, SiO_4^{4-} units are replaced with AlO_4^{5-} tetrahedra and the charge is balanced by the incorporation of Li^+. We removed three Li ions, changed two oxygens to carbons, discarded one of the Al atoms and replaced all the remaining cations with Si. We obtained a symmetrical crystalline model with composition $Si_5C_2O_6$: $(SiC)_2(SiO_2)_3$. Figure 2.2.

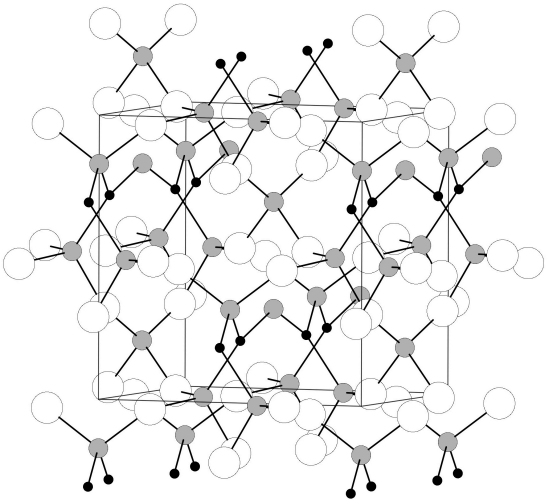

Figure 2.2. Ball-and-stick model of $Si_5C_2O_6$ (2:3). Grey circles are Si, black circles C, and unfilled are O. Structure shows distribution of SiC_xO_{4-x} tetrahedra along with two-fold coordinated O and trigonal planar carbon.

A SiCO model with 22mol% SiC was constructed from $(SiC)_2(SiO_2)_3$ model shown in Figure 2.2. We took $Si_5C_2O_6$ structure and doubled the unit cell to get $Si_{10}C_4O_{12}$, where two carbons were changed to oxygen atoms and one Si was removed. All the hand-crafted models are listed in Table 3.3.

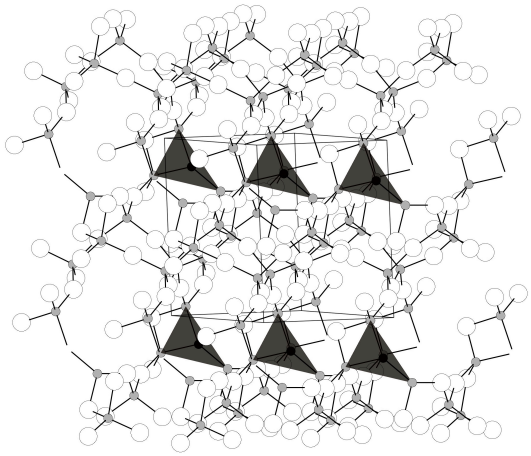

Figure 2.3. Model of Si_7CO_{12} (1:6) with the emphasis on trigonal planar carbon shown in a polyhedral view. Grey circles are Si, black circles C, and unfilled are O.

2.4 Density functional theory computations

Structures and energies of all structural models are computed within density functional theory (DFT) [17]. We employ the VASP-code [24-27], which implements the pseudopotential method together with plane-wave basis sets. The DFT calculations consist of two steps. First, all the models generated with AIRSS are initially optimized with a reduced k-point set (2x2x2). In the second step, the best-chosen crystalline structures are optimized with a larger number of k-points to ensure the appropriate convergence of energy differences and structural data. We rely on the Generalized Gradient Approximation (GGA) [25] and use a cut-off of 500 eV for the expansion of the wave function into a plane wave basis set. The final k-point grids effectively sample the Brillouin zone with a resolution of at least $2\pi*0.04Å^{-1}$.

Reference calculation of α-quartz SiO_2, β-SiC and graphite yielded energies of -24.004 eV, -15.154 eV and -9.200 eV per formula unit, respectively. The excess energy of a model is computed with the following formula: $\Delta E_{excess} = 1/(x+y)(E_{model} - (xE(SiO_2) + yE(SiC) + zE(graphite)))$, ΔE_{excess} refers to the excess energy per Si atom. In the case of the stoichiometric models graphite is excluded from the equation. In the following section we report our results referring to them as enthalpy of formation. For the enthalpy we have H = E + PV, where the term PV is ignored since all the calculations are performed at zero pressure and there is no significant change in volume. Hence the terms excess energy and enthalpy are used interchangeably.

CHAPTER 3

MODELING RESULTS

3.1 Stoichiometric SiCO

This work presents SiCO crystalline structures, their composition, thermochemistry, crystallographic description, and energetic stability compared to amorphous models. An overview of the structures with lowest energy is given in Table 1. We include the binary phases β-SiC and SiO_2 (quartz), since they are the end members of the SiO_2-SiC tie-line. Before we discuss energies listed in Table 3.1 and their implications on the feasibility of ternary crystalline SiCO, we focus on a description of the different structures.

Table 3.1 The lowest energy configurations for the given compositions generated with AIRSS.

Structures	Volume {Å^3} per Si	Energy {eV} per Si	Space group	SiC, mol%	SiO_2, mol%	E_{excess} {eV} per Si
$Si_3C_2O_2$, $(SiC)_2(SiO_2)_1$	27.70	-17.830	*P*21 (4), *Z*=2	66.67	33.33	0.275
Si_2CO_2, $(SiC)_1(SiO_2)_1$	33.80	-19.300	*I*4*mm* (107), *Z*=8	50.00	50.00	0.284
Si_3CO_4, $(SiC)_1(SiO_2)_2$	33.70	-20.650	*Cm* (8), *Z*=2	33.33	66.67	0.404
Si_4CO_6, $(SiC)_1(SiO_2)_3$	33.30	-21.440	*R3* (146), *Z*=3	25.00	75.00	0.352
Si_5CO_8, $(SiC)_1(SiO_2)_4$	37.86	-21.917	*P* 1 (1), *Z*=1	20.00	80.00	0.317
Si_7CO_{12}, $(SiC)_1(SiO_2)_6$	39.60	-22.320	*P* 1 (1), *Z*=1	14.29	85.71	0.417
$Si_{10}CO_{18}$, $(SiC)_1(SiO_2)_9$	43.86	-22.750	*P* 1 (1), *Z*=1	10.00	90.00	0.368
β-SiC	20.89	-15.154	*F* -4 3 *m* (216), *Z*=4	100.00	0.00	0.00
q-SiO_2	40.74	-24.004	*P* 3_2 21 (154), *Z*=3	0.00	100.00	0.00

Overall, we investigated about 10,000 structures generated by AIRSS, more than 1,000 for each composition. This method has been used to successfully predict the ground state structures of a number of systems [29]. The graph in Figure 3.1 shows examples of how the

energy is distributed during the structure search process for the compositions Si_2CO_2 and Si_4CO_6.

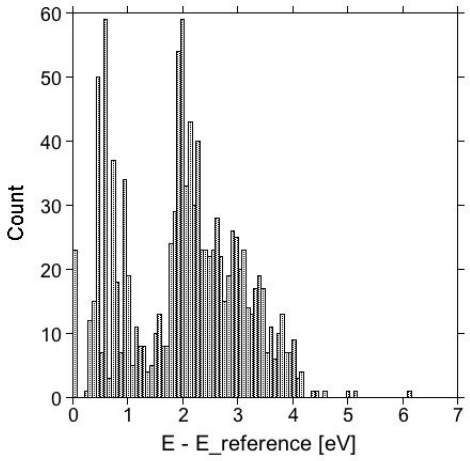

(a)

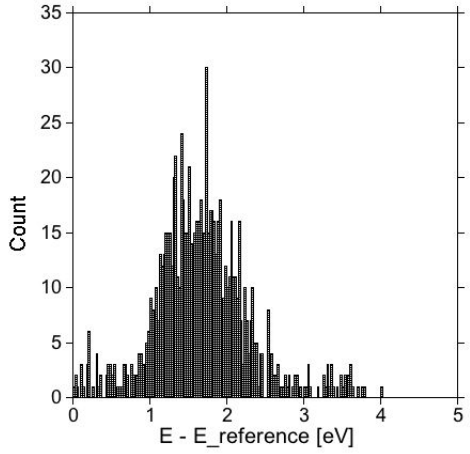

(b)

Figure 3.1 Distribution of energies for Si_2CO_2 (a) and Si_4CO_6 (b) structure type search

In Figure 3.1 are unique energy distributions for two different compositions. For the Si_2CO_2 energy search the highest count of structures is at about 0.6 eV and 2 eV. These are the structures that are found very often and show a particular structural configuration that we would like to refer to as “attractor”. In an energy-surface picture, they constitute the local minimum for a rather large area on the potential surface. Each model that is created in this area is optimized to the same “attractor” and since it is a random process, the proportion of equivalent models corresponds simply to a relative measure of the area associated to this model [23]. An example of an “attractor” structure Si_2CO_2 is shown in the Figure 3.2 below.

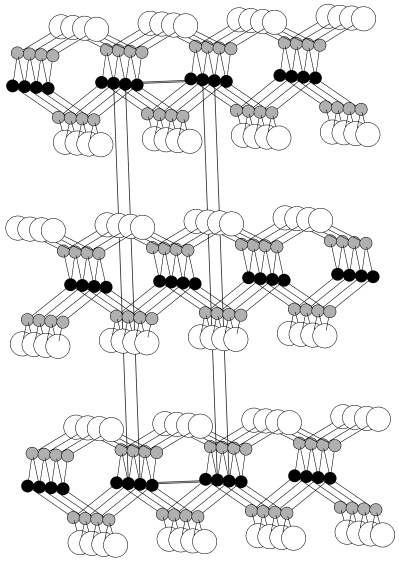

Figure 3.2 Ball-and-stick model of Si_2CO_2 (1:1). Grey circles are Si, black circles C, and unfilled are O. The structure exhibits layered pattern with β-SiC oxidized at its (100) surface.

Structures we find with the lowest energy for a given composition have basic motifs in common: Si is four-fold coordinated, approximately tetrahedral, bonding to C and O. We denote these so-called “mixed tetrahedra” as SiC_xO_{4-x} (x=0,1,2,3,4), with x carbon and 4-x oxygen neighbors to Si. Carbon is four-fold coordinated to Si, approximately forming CSi_4-tetrahedra and oxygen bonds to two Si atoms. Reported NMR ^{29}Si and ^{13}C NMR studies of amorphous

SiCO indicate a random network structure with $SiC_xO_{(4-x)}$ tetrahedra and carbon appears in its sp^3-C form [8, 20, 30]. Our lowest energy structures thus agree with results from NMR. The following model of SiCO with 50 mol% of SiC, shown in Figure 3.3, illustrates these features.

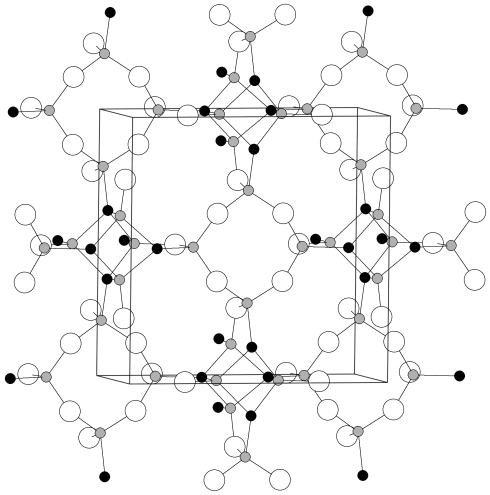

Figure 3.3. Ball-and-stick model of the lowest energy configuration for Si_2CO_2 (1:1). Grey circles are Si, black circles C and unfilled are O. Spacious voids are formed within the structure due to corner-shared tetrahedral network of Si.

The structure in Figure 3.3 is described by carbon tetrahedra sharing edges that form one-dimensional chains or rods. The “carbide” rods are connected via “oxide” tubes. In a projection along the rod or tube direction, the two entities form a simple square pattern.

A typical family of ternary SiCO structures we encounter has “oxidized” SiC surfaces as shown in Figure 3.4. These structures are characterized by slabs of either α-SiC or β-SiC exposing Si-terminated surfaces, with O atoms bridging between Si atoms on the surface to saturate dangling bonds. Due to the “construction”, Si and C atoms are almost regular tetrahedrally coordinated. Since the SiC slabs may vary in their thickness, such models are of particular interest towards the SiC edge of the composition diagram, for high SiC-content. We note that the oxidized β-SiC (100) surface, with each one O bridging between two Si, is a known subject in materials chemistry [31].

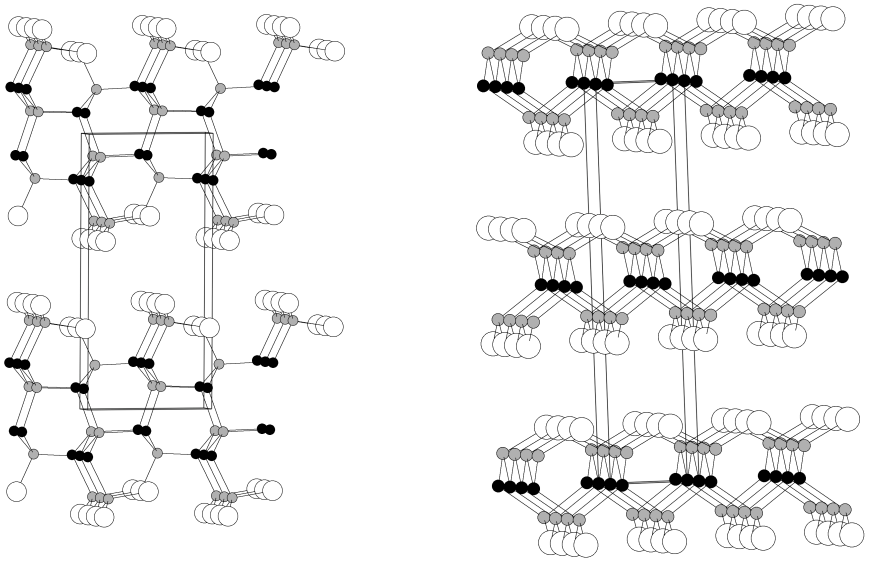

(a) (b)

Figure 3.4 (a) Ball-and-stick model of $Si_3C_2O_2$ (2:1). Grey circles are Si, black circles C, and unfilled are O. Structure exhibits layered pattern with oxidized SiC at (1 -1 0) surfaces. (b) Carbon tetrahedra within Si_2CO_2 (1:1) forming channels of tetrahedra connected at the corners; this structure is related to β-SiC when oxidized at its (100) surface.

As an example, we show a structure with 66%-mol content of SiC in Figure 3.4 (a). It is related to wurtzite SiC when oxidized at the (1 -1 0) surface. Figure 3.4 (b) shows oxidized β-SiC at its (100) surface.

Structures with high SiC content exhibit CSi_4-tetrahedra sharing vertices or edges. Towards the SiO_2-rich side of SiCO the CSi_4-tetrahedra get more “diluted” within the SiO_2 phase. The first appearance of isolated CSi_4-tetrahedra is observed in structures with 25%-mol content SiC. Figure 3.5 shows the lowest energy configuration we found for 25%-mol content SiC. Interestingly, this structure exhibits a cubic closed packing of anions, with C and O ordered over the anion positions. Si atoms fill 2/7 of the available tetrahedral sites.

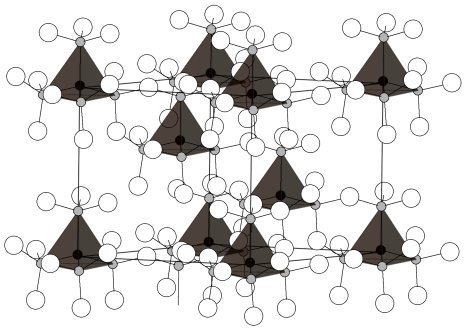

Figure 3.5. Isolated carbon tetrahedra within Si_4CO_6 (1:3) structure.

Figure 3.6 (a) displays the lowest energy structure of Si_5CO_8 (20%-mol content SiC). The structure is characterized by CSi_4-tetrahedra arranged in layers, with O atoms bridging between tetrahedra both in-plane and between different layers. In this model we observe a structural relationship to the mineral sinoite, Si_2N_2O. In Si_2N_2O crystal structure the layers of SiN_3O tetrahedra are also connected through oxygen atoms. Furthermore, this structure of sinoite turned out to be an excellent host lattice for the incorporation of calcium cations with the resulting structure of $Ca(Si_2O_2N_2)$ [32], which is important for its photoluminescent properties [33]. Both structures Si_5CO_8 and Si_2N_2O are shown in Figure 3.6.

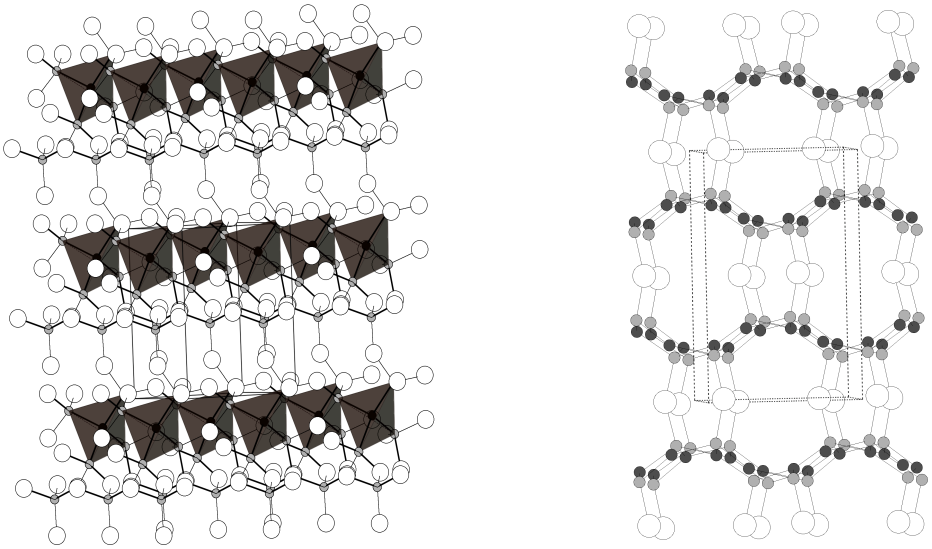

(a) (b)

Figure 3.6. (a) Isolated carbon tetrahedra within Si_5CO_8 (1:4) structure. (b) is Si_2N_2O where grey circles are Si, dark grey circles refer to N atoms and plain white ones are oxygens.

Figure 3.7 displays Si_7CO_{12} (14 mol-% SiC) generated with USPEX, which we obtained as the lowest energy structure for this composition. This structure is characterized by isolated tetrahedra of CSi_4 connected via SiO_4 units. All the atoms satisfy a "perfect" coordination within the SiCO network.

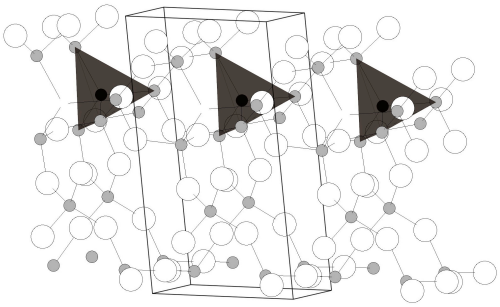

Figure 3.7. The lowest energy configuration of Si_7CO_{12} (1:6) structure. Isolated tetrahedra of CSi_4 units are in one plane and shown in a polyhedral view.

Table 3.1 summarizes the data for lowest energy structures for each composition. It includes energy and volume we computed for the corners of the SiC-SiO_2 tie-line, β-SiC and quartz-SiO_2. Of particular interest is the excess energy ΔE_{excess} of each structure. To compute ΔE_{excess}, of a structure with composition $Si_{x+y}C_xO_{2y}$, we subtracted the appropriate energies for the amounts of SiC and SiO_2 from the total energy of $(SiC)_x(SiO_2)_y$, and referenced the excess per Si atom accordingly, $\Delta E_{excess} = 1/(x+y)\ (E_{model} - (xE_{SiO2} + yE_{SiC}))$. Note that, our choice of reference then corresponds to 2 atoms for SiC, but for 3 atoms in case of SiO_2.

The data shows that excess energies are positive for every composition we investigated. This result implies that a decomposition of the ternary structures into binaries SiC and SiO_2 is exothermic at ambient pressure. Neglecting entropy contributions, therefore, none of the ternary SiCO structures we investigated is thermodynamically stable. The lack of a stable ternary structure supports XRD results, which did not reveal a ternary crystalline SiCO [12]. Note that in the ternary system SiNO, the mineral name sinoite Si_2N_2O, is well known [34]. Sinoite structure and even some high-pressure polymorphs have been investigated earlier [35]. The data for ΔE_{excess} is plotted as a function of mol-% SiC and shown in Figure 3.8.

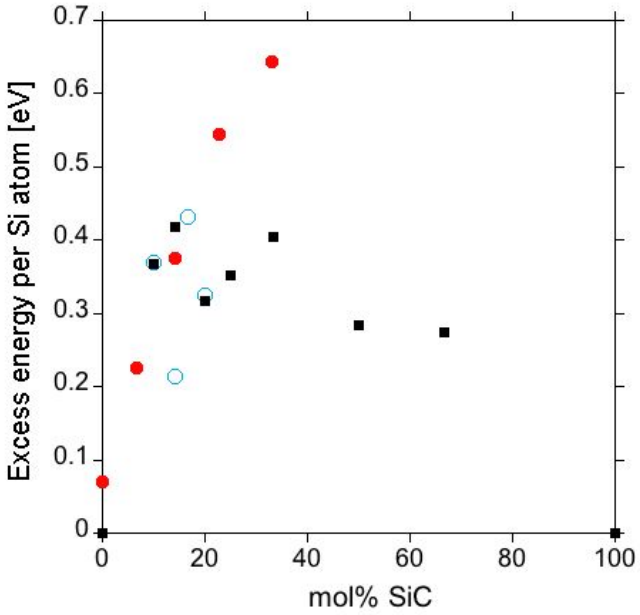

Figure 3.8. Plot of the excess energy per Si atoms as a function of mol% SiC within SiCO. Red circles represent amorphous models of SiCO [14]. Black squares correspond to the crystalline structures generated with AIRSS. Hollow circles represent crystalline structures generated by USPEX. For each composition we show only the lowest energy model.

The energy results from USPEX (Table 3.2) appear to closely match the results from AIRSS. In Figure 3.8 data points from USPEX overlap or lie close to data points reported by AIRSS. The exception is the structure of Si_7CO_{12} that turns out lower in excess energy than any other models. However, there is no specific trend observed for the crystalline structures produced by two different methods.

Table 3.2 The lowest energy configurations for the given compositions generated with USPEX.

Structures	Volume {Å^3} per Si	Energy {eV} per Si	Space group	SiC, mol%	SiO_2, mol%	E_{excess} {eV} per Si
Si_5CO_8, $(SiC)_1(SiO_2)_4$	35.44	-21.910	*P* 1 (1), Z=1	20.00	80.00	0.325
Si_6CO_{10}, $(SiC)_1(SiO_2)_5$	39.43	-22.100	*P* 1 (1), Z=1	16.60	83.40	0.431
Si_7CO_{12}, $(SiC)_1(SiO_2)_6$	36.56	-22.530	*P* 1 (1), Z=1	14.29	85.71	0.214
$Si_{10}CO_{18}$, $(SiC)_1(SiO_2)_9$	43.86	-22.750	*P* 1 (1), Z=1	10.00	90.00	0.368
β-SiC	20.89	-15.154	*F* -4 3 *m* (216), Z=4	100.00	0.00	0.000
q-SiO_2	40.74	-24.004	*P* 3_2 21 (154), Z=3	0.00	100.00	0.000

The overview of all hand-crafted models, their structural compositions and lowest energies are reported in Table 3.3. The discussion of the results can be found in Sec. 4.1.

Table 3.3 The lowest energy configurations for the given compositions of the hand-crafted models.

Structures	Volume {Å^3} /f.u.	Energy {eV} per f.u.	Space group	SiC, mol%	SiO_2, mol%	E_{excess} {eV}
$Si_{80}CO_{158}$, $(SiC)_1(SiO_2)_{79}$	3150.26	-1902.120	*C* 1 2 1 (5), Z=1	1.25	98.75	9.350
$Si_{25}C_2O_{46}$, $(SiC)_2(SiO_2)_{23}$	1077.27	-571.765	*P* 1 (1), Z=1	8.00	92.00	10.635
Si_7CO_{12} , $(SiC)_1(SiO_2)_6$	309.72	-155.265	*P* 1 (1), Z=1	14.29	85.71	3.913
$Si_9C_2O_{14}$, $(SiC)_2(SiO_2)_7$	325.18	-192.233	*P* 1 (1), Z=1	22.00	78.00	6.103
$Si_{10}C_4O_{12}$, $(SiC)_2(SiO_2)_3$	330.57	-197.433	*C* 1 2 1 (5), Z=2	40.00	60.00	3.603
β-SiC	20.89	-15.154	*F* -4 3 *m* (216), Z=4	100.00	0.00	0.00
q-SiO_2	40.74	-24.004	*P* 3_2 21 (154), Z=3	0.00	100.00	0.00

3.2 SiCO with excess carbon

As mentioned in the introduction, the polymer-to-ceramic method allows for the incorporation of significant amounts of carbon into SiCO ceramics. Therefore, a detailed picture of the atomistic structure of SiCO with excess carbon is desirable and can help in further understanding of properties such as resistance to crystallization of this material, its viscoelastic

and creep behavior. Unlike silica, SiCO resists crystallization at high temperature, which is attributed to the presence of carbon in the material. Multiple experiments reported the bonding environments associated with the presence of carbon in the material. ^{29}Si NMR studies have indicated that the carbon in SiCO exists in mixed SiC_xO_{4-x} tetrahedra of silicon [36]. ^{13}C NMR results indicated sp^2-bonded carbon environments like in graphite and carbons with cubic site symmetry as in sp^3-bonded carbon in SiC units [30]. Raman spectroscopy suggests the presence of graphene sheets [37]. And, HRTEM reports by Kleebe *et al* have furthermore indicated the presence of graphitic carbon in nanoscale units [7]. Infrared spectra did not show vibrations due to carbon-oxygen bonds; therefore, carbon has bonds either to silicon or to itself, but not to oxygen [39].

The concept of nanodomains within the material is well addressed in Ref. [21], yet the detailed atomistic description remains obscure. Nevertheless, there are claims that according to this nanodomain structure, SiCO material exhibits high temperature stability and resistance to crystallization and even the thermodynamic stability is mostly attributed to this nanodomain character of the material [22].

Previous modeling work has addressed structure and energetics of the “free” carbon phase for the amorphous models of SiCO [14]. The lowest energy structures were found in models where the carbon phase was not bonded to the glass phase, but instead segregated in the form of graphene sheets. If, on the other hand, carbon segregation appeared to be bonded covalently to the glassy phase it would cause models to exhibit large excess energy [14]. In conclusion, previous modeling results could not indicate any favorable interface between the glassy phase of SiCO and ‘free’ carbon phase. Even though it appears like there is a solid base for the structural trends in amorphous SiCO ceramics, an explanation for the negative enthalpy of formation for this material has not yet been provided.

This section presents SiCO crystalline approximants with excess carbon, their crystallographic description, and energetic stability compared to amorphous models and

stoichiometric crystalline structures discussed in the previous section. An overview of our structures with lowest energy is given in Table 3.4. We include the binary phases β-SiC, SiO_2 (quartz) and graphite, and give the calculated excess energy per "free" carbon. In order to calculate this value, we used the following formula: ΔE_{excess}per "free" carbon =1/z ((E($Si_{x+y}C_xO_{2y}$ + zC))-(E($Si_{x+y}C_xO_{2y}$))), where $Si_{x+y}C_xO_{2y}$ is a crystalline stoichiometric model of a same size. Note that we compute the excess energy "per carbon" with reference to a ternary crystalline SiCO (Section 3.1) to see the impact of the additional carbon on the energetics. Before we discuss energies listed in Table 3.4 and their implications on the feasibility of ternary crystalline SiCO, we focus on a description of the different structures.

Table 3.4 The lowest energy configurations for the given compositions of the SiCO + C_{free} models.

Structures	Volume {Å^3} per Si	Energy {eV} per Si	E_{excess} {eV} per Si	E_{excess} {eV} per "free" carbon
$Si_2C_2O_2$, $(SiC)_1(SiO_2)_1$ +C	35.00	-23.420	0.750	0.940
$Si_2C_3O_2$, $(SiC)_1(SiO_2)_1$ +2C	40.90	-27.770	1.000	0.720
$Si_4C_2O_6$, $(SiC)_1(SiO_2)_3$ +C	40.00	-23.490	0.590	0.840
$Si_5C_3O_8$, $(SiC)_1(SiO_2)_4$ +2C	43.10	-24.780	1.130	1.030
$Si_5C_5O_8$, $(SiC)_1(SiO_2)_4$ +4C	42.00	-27.750	1.840	0.480
β-SiC	20.89	-15.154		
q-SiO_2	40.74	-24.004		
$C_{graphite}$	-9.20 per C atom			

Structures with lowest energy have basic motifs in common: Si is four-fold coordinated, approximately tetrahedral, bonding to C and O, oxygen is always linear bonded to Si atoms only. Carbon is in four-fold coordination when it is bonded to Si atoms, hence a CSi_4 unit, with the local environment being approximately tetrahedral, so called sp^3-carbon. When carbon bonds to itself, it's predominantly trigonal planar, or sp^2. These observations agree with NMR results that also confirmed tetrahedral CSi_4 units and sp^2-carbon [8, 30]. The crystalline models

reflect the structural trends discussed above and the structure with the composition of Si_2CO_2 + C is shown in the Figure 3.9.

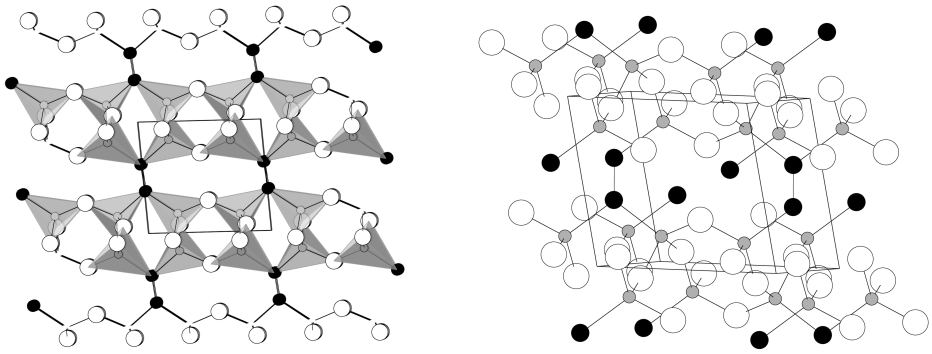

(a) (b)

Figure 3.9 The lowest energy configuration for Si_2CO_2 +1C. Grey circles are Si, black circles C and unfilled are O. (a) Silicon atoms are depicted in the polyhedral form. (b) is a ball-and-stick representation of the same model with the emphasis on carbon atoms.

Figure 3.9 shows the common motifs of the SiCO network: mixed tetrahedra of Si, sp^2-carbon has two bonds to Si and one to C. The structure appears layered connected via carbon dimers.

A model with the composition Si_2CO_2 +2C can be found in Figure 3.10. In this structure Si appear only in SiC_2O_2 tetrahedra. All oxygens are divalent and the carbon atoms appear as linear C_3^{4-}.

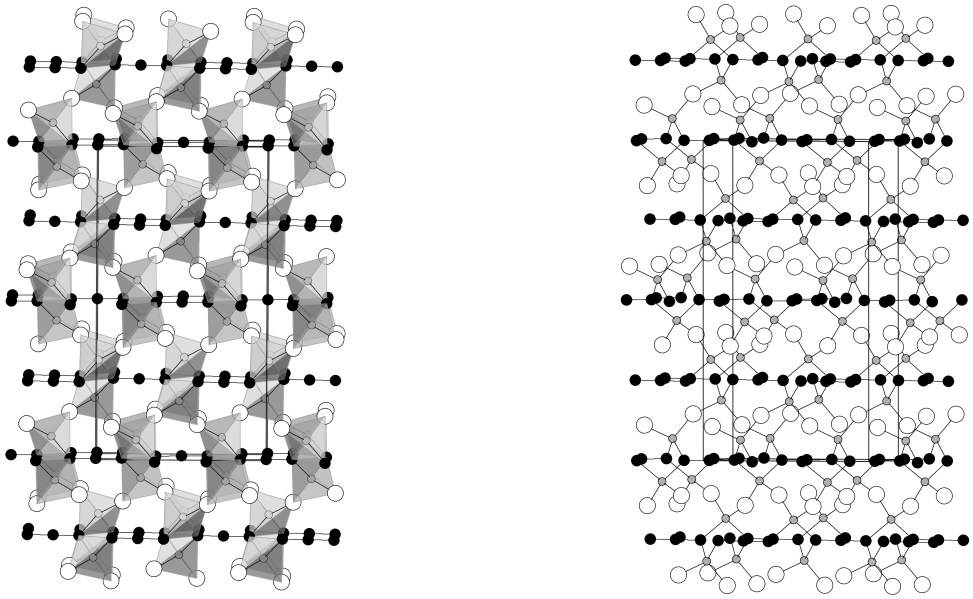

(a) (b)

Figure 3.10 The lowest energy configuration for Si_2CO_2 +2C. Grey circles are Si, black circles C and unfilled are O. (a) Silicon atoms are depicted in the polyhedral form. (b) is a ball-and-stick representation of the same model.

The composition of the model in Figure 3.11 is Si_4CO_6 +1C. Carbon atoms are three-fold and four-fold connected and form a four-carbon chain. Figure 3.11 (b) is the top view of the structure that clearly shows carbon connectivity.

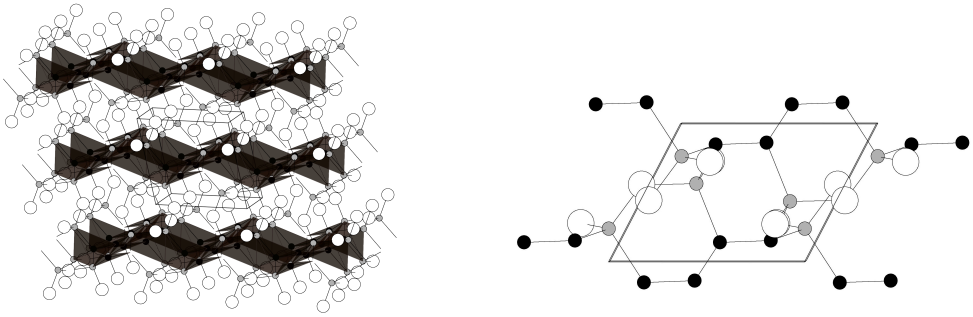

(a) (b)

Figure 3.11 The lowest energy configuration for Si_4CO_6 +1C. Grey circles are Si, black circles C and unfilled are O. (a) Carbon atoms are depicted in the polyhedral form. (b) is a ball-and-stick representation of the same model.

Figure 3.12 shows a structure with 20 mol% SiC and with 2 carbons added: $(SiC)_1(SiO_2)_4$ + 2C. Carbon atoms are two-fold and three-fold connected arranged in dimers. The layers of the structure are bridged with four-carbon rings and dimers alternating throughout the network that can be seen in Figure 3.12 (b).

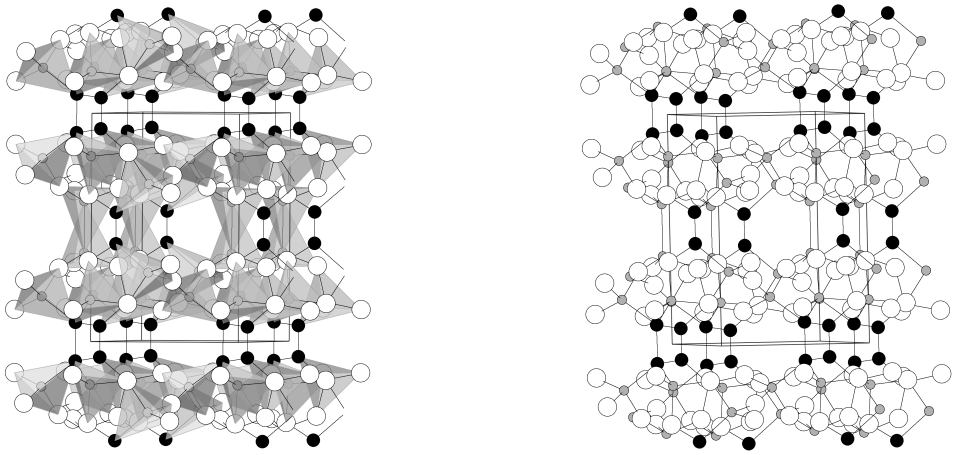

(a) (b)

Figure 3.12 The lowest energy configuration for Si_5CO_8 +2C. Grey circles are Si, black circles C and unfilled are O. (a) Silicon atoms are depicted in the polyhedral form. (b) is a ball-and-stick representation of the same model.

The last model from Table 3.4 is Si_5CO_8 +4C. In this model various silicon tetrahedra are observed: $SiCO_3$, SiC_2O_2 and SiC_3O. As for the carbon atoms, the majority is four-fold connected with some three-fold connected carbons as well. This structure can be found in Figure 3.13.

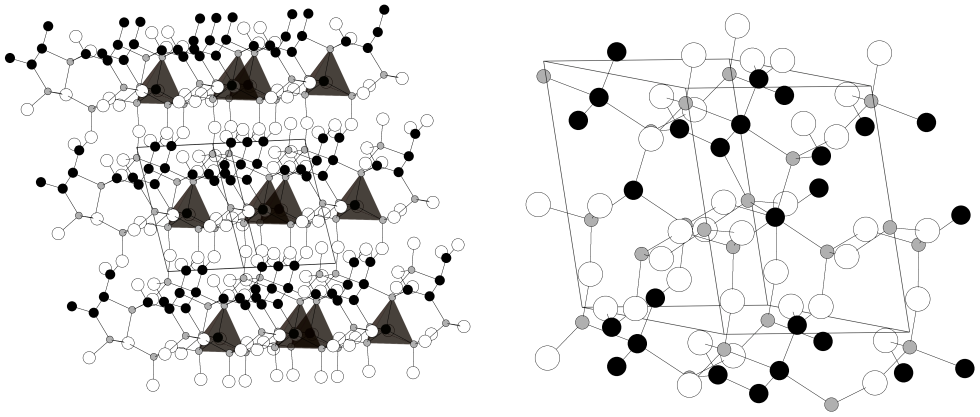

(a) (b)

Figure 3.13 The lowest energy configuration for Si_5CO_8 +4C. Grey circles are Si, black circles C and unfilled are O. (a) CSi_4 units are shown in the polyhedral form. (b) is a ball-and-stick representation of the same model.

In this structure the four-fold connected carbon appears in CSi_4 units, which has not been observed in previous models with excess carbon but which is typical for stoichiometric SiCO models.

Summarizing structural trends for all the models described above, it is important to highlight the similar behavior of carbon bonding. Carbon as a “free” phase prefers to bond to itself, which primarily results in the formation of dimers and trimers. This onset of π-bonded units may eventually extent to graphite.

The data of Table 3.4 is combined with the data for stoichiometric SiCO (Figure 3.8) into Figure 3.15. Thus Figure 3.15 combines excess energies for all three sets of SiCO models: stoichiometric amorphous and crystalline SiCO as well as SiCO with excess carbon.

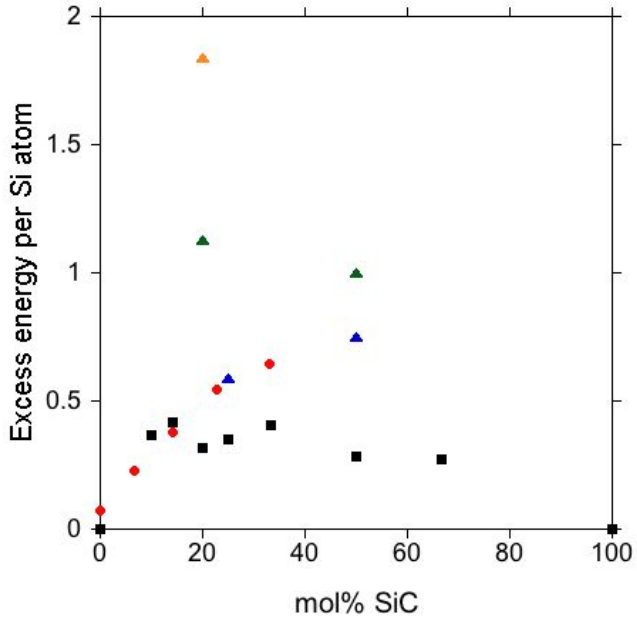

Figure 3.14 Plot of excess energy as function of mol% SiC within SiCO. Red circles represent amorphous models of SiCO [14]. Black squares correspond to the crystalline structures generated with AIRSS. Blue triangles refer to the structures with one additional carbon; green triangles-two additional carbons and orange triangle corresponds to four additional carbons.

All models with additional carbon exhibit a substantial excess energy (Table 3.4) as shown in Figure 3.14. Looking at the structure $(SiC)_1(SiO_2)_1$ +1C, the excess energy per Si comes out to be 0.75 eV and upon doubling the amount of carbon the resulting excess energy is 1.00 eV. This observation helps to understand the structural trends of the models with excess carbon. When one additional carbon is first introduced to the system, it forms bonds with two Si atoms and one carbon; upon adding another carbon to the same system, it inserts itself between two carbon thus avoiding bonds to Si. As a result, in Figure 3.9 the dimers of carbon are formed and in Figure 3.10 we already observe carbon trimers. Therefore carbon to silicon bonds are less favored over carbon-to-carbon bonds. The “free” carbon phase separates from

the rest of the glassy matrix as was already reported as a common characteristic of these materials [7, 14].

Table 3.4 reports the excess energy per "free" C atom which comes out to ~ 1 eV. This significant "penalty" can be attributed to the formation of a C-**C-Si**-O interface [14]. Nevertheless, Varga *et al* attribute the thermodynamic stability of some amorphous SiCO to the presence of graphene-silica interface and the presence of macroscopic crystalline silicon mixed tetrahedra [22]. In contrast, our work does not find any favorable interface formation between the glassy phase and the "free" carbon phase.

In summary of the results from structural modeling, the following conclusions are made regarding the additional carbon incorporation into the SiCO network. The excess energy was calculated from the difference between the models and the appropriate combination SiC, SiO_2 and graphite. A substantial excess energy is observed for all models with additional carbon and this excess energy is larger compared to the stoichiometric models of SiCO.

This increase in energy is attributed to the unfavorable formation of both C-Si and C-O bonds. C-O bonds were found in $Si_5C_3O_8$ (Figure 3.12) and $Si_5C_5O_8$ (Figure 3.13) models. Unfortunately, we cannot differentiate between the energetic "penalties" that come from each new bond that was formed. For the models that did not have C-O bonds, we could attribute excess energy to the unfavorable formation of C-**C-Si**-O bonding interface that takes ~0.8 eV to create per bond. We find a correlation with the previously reported results for the amorphous models that attribute excess energy per carbon atom to the formation of C-**C-Si**-O interface, which takes an additional ~ 1eV to make [14].

With the crystalline structures we indeed obtained a more comprehensive picture of structural possibilities for amorphous SiCO with excess carbon. While previous amorphous models gave an account of structural arrangement between "free" carbon phase and the glassy matrix [14, 16], there were several limitations of that approach. Amorphous models require a large number of atoms for a single structure, which in turn limits the number of models one can

construct and investigate, due to high computational costs. Another limitation has to do with the way these models were generated, which also introduced a significant amount of bias. The local coordination of all atoms was already predefined; all the structures exhibited perfect chemical order- only Si-O and Si-C bonds. In order to simulate the “free” carbon phase in amorphous models, fragments of either graphite or graphene were inserted into the structure by hand. Nevertheless, the results from amorphous modeling served as a reference and comparison point for this work.

Crystalline models, on the other hand, are much faster to generate since only few atoms are required in a crystal structure. None of the bonding environments were predefined for the thousand of structures that were generated, which tremendously reduced the amount of bias in this method. With the obtained results we were able to trace bonding patterns in stoichiometric SiCO as well as bonding preferences of “free” carbon in SiCO.

It should be noted that energies reported in Table 3.4 do not support negative enthalpy of formation, as reported for some amorphous SiCO ceramics [22]. Structural modeling did not show any indication of negative enthalpy of formation upon insertion of additional carbon.

CHAPTER 4

DISCUSSION AND SUMMARY OF SICO STRUCTURAL MODELING

4.1 Discussion of structural modeling.

The results obtained from generating crystalline approximants of SiCO address two major issues of these amorphous ceramics: structural trends and thermochemistry. For the stoichiometric glass phase of SiCO with composition $SiC_xO_{(2-2x)}$(=xSiC+ (1-x)SiO_2), thus without additional so-called "free" carbon, the concept of a perfect network holds for the composition with up to 33 mol% SiC. This concept of "perfect network" has been addressed multiple times in experiments [20, 40] and in previous work on amorphous SiCO models [14, 15]. Here in this study, a much wider range of compositions of SiCO starting from 10 mol % to ~66 mol % of SiC is presented. Fulfilling expectations, all crystalline structures with lowest energy appear sound, exhibiting tetrahedrally coordinated Si and C besides two-fold coordinated O. Though sometimes edge-sharing between tetrahedra is observed the models appear to be mixtures of crystalline SiC and SiO_2. These results agree with ^{29}Si NMR experiments supporting SiO_xC_{4-x} mixed tetrahedra as well as with ^{13}C NMR reporting CSi_4 units [41].

None of the lowest energy stoichiometric models show C-O or C-C bonding, nor do they exhibit sp^2-C. Thus, under the constraint of composition (SiO_2:SiC) any such bonds, Si-Si, C-C, or C-O, will occur only with significant energy penalty. In $(SiC)_2(SiO_2)_3$ and $(SiC)_2(SiO_2)_7$ models we created such "bad" bonds, C-O and Si-Si. The energetic penalty estimated per "bad" bonds came down to ~ 1.7 eV.

Thus, a SiCO network will consist of Si-O and Si-C bonds only. However, one may think that a CSi_3-units with sp^2 carbon may be present in a structure. Since one link towards the Si is lost that way, it should be compensated by OSi_3 units. However, after optimization the structure has under coordinated Si atoms, hence SiO_3 units. As a result of this distortion, this model has an excess energy is ~6 eV with respect to crystalline SiC and SiO_2, Figure 4.1.

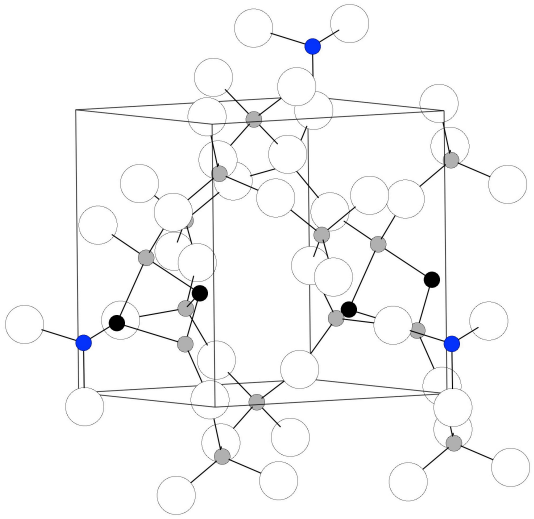

Figure 4.1. Ball-and-stick model of $Si_9C_2O_{14}$ (2:7). Grey circles are four-fold connected Si, blue circles are three-fold connected Si, black circles C, and unfilled are O. Structure shows three-fold connected sp^2-C and SiO_3 units.

The modeling was extended by including excess carbon into stoichiometric SiCO models resulting in a general composition $SiC_xO_{(2-2x)}C_y$ including Si-C, Si-O and C-C bonds. All the models fulfilled the expectations, exhibiting tetrahedrally coordinated Si and two-fold coordinated oxygen atoms. Carbon atoms arrange as dimers and trimers with three-fold connected carbon being more dominant than four-fold connected sp^3-carbon. This carbon arrangement can be related to graphite, the common form of carbon found within amorphous SiCO. The structural trends of our crystalline structures agree with NMR experiments, which gives us confidence in the validity of our approach [20].

Screening more than 10,000 models, we find that all ternary structures exhibit positive enthalpy of formation. Overall, we don't find any indication for a thermodynamically stable SiCO ceramic despite the fact that all our structure appear sound and satisfactorily reflect the structural trends of SiCO. Thus our results do not support a negative enthalpy of formation as reported for some a-SiCO ceramics [22]. Varga *et al* speculates that this thermodynamic stability of some amorphous SiCO is due to the presence of nanodomains, which by definition

have a large number of interfaces. We have investigated vast possibilities of these interfaces within the SiCO system but could not confirm any favorable interface formation. Our discussion does not include the influence of hydrogen on the stability of this material. Yet a preliminary modeling indicates that only small quantities of hydrogen, 1-5 atom-%, will be sufficient to explain these puzzling experimental results [14].

The structures that are reported here are likely to lie on or close to the global energy minimum. While one cannot be sure that the true lowest energy models were found, AIRSS has proved to be successful in predicting structures, which have subsequently been varied by experiments [29]. The USPEX code has been used to successfully predict new stable compounds [42, 43]. This experience together with the sound structural data and the smooth trends in energy of the best configurations provides the confidence that a particularly "stable" configuration was not missed. Note that we performed searches for unit cell containing up to 80 atoms and did not choose highly restrictive conditions. In one case, for $(SiC)_1$:$(SiO_2)_1$, the lowest energy structures emerged with 20 atoms in the primitive unit cell (Table 3.1).

4.2 Summary of modeling results

A wide range of compositions of crystalline models for SiCO ceramics addressing structure and energy is presented in this work. A database of crystalline models was generated with the structure search codes AIRSS and USPEX. We added handcrafted models that did not quite reflect the "perfect" bonding environment of SiCO, but instead included such elements as three-fold connected carbon and silicon atoms. With these handcrafted models we were able to look at alternative bonding scenarios and study associated energies.

All models well support previously reported NMR results: SiC_xO_{4-x} mixed tetrahedra and CSi_4 units represent the main features of SiCO ceramics. As for the "free" carbon phase, three-fold and four-fold connected carbon observed in the models corroborate the common conception of excess carbon in amorphous SiCO and agree with results from Raman spectroscopy [11, 12]. We are confident that our crystalline models yield a manifold of possible

bonding environments within amorphous SiCO. We did not find any indication for the stability of the ternary phase of SiCO with respect to its binary compounds, q-SiO_2, β-SiC and to graphite. Thus our results do not support a negative enthalpy of formation of a-SiCO. A “free” carbon phase bonded to the SiCO destabilizes crystalline structures even more and no favorable interface formation was observed.

The goal of this work was to obtain a detailed microscopic picture of structural trends in amorphous SiCO and to assist in the interpretation of structure-thermochemistry relationship of this material. Summarizing the contributions of this work we obtain:

- Our crystalline models provided a comprehensive picture of structural possibilities in SiCO exceeding previous modeling efforts using amorphous models.
- Our result did not indicate that the occurrence of mixed SiC_xO_{4-x} tetrahedra has a favorable effect on the enthalpy of formation of SiCO. Every single crystalline model in this work has units of SiC_xO_{4-x}.
- With the presence of excess carbon, our models became even more unstable and we could attribute the reason for this instability to the formation of C-**C-Si**-O bonding interface.

The database of crystalline SiCO structures we generated in this work can help to better understand the nature of the structural heterogeneity in amorphous SiCO. This knowledge of the structure is crucial in understanding a wide range of properties such as conduction, nucleation, crystallization and mechanical properties such as creep and viscoelasticity. The ultimate goal is to study this amorphous material and to have a definite understanding of the relationship between composition, microstructure and properties. With this knowledge we can control material’s properties for specific applications.

APPENDIX A

CRYSTALLINE STRUCTURE DESCRIPTIONS

AIRSS crystal structures description (Table 3.1)

$Si_3C_2O_2$; Spgr.: *P* 2_1 (4), Z=2; a=11.1629, b=5.0178, c=2.9831, β=96.386

atom	W	x	y	z
Si	2a	0.3204	0.1284	0.6331
Si	2a	0.0827	0.0906	0.0344
Si	2a	0.8397	0.0924	0.4338
C	2a	0.0773	0.4679	0.0316
C	2a	0.8321	0.4658	0.4301
O	2a	0.2958	0.4537	0.6214
O	2a	0.6153	0.5624	0.8401

Si_2CO_2; Spgr.: *I*4*mm* (107), Z=8 a=10.3995, c=4.9967

atom	W	x	y	z
Si	8d	0.3805	0	0.6558
Si	8d	0.2119	0	0.1233
C	8d	0.6284	0	0.2812
O	8c	0.8716	0.8716	0.1947
O	8d	0.2386	0	0.7958

Si_3CO_4; Spgr.: *Cm* (8), Z=2; a=9.5193, b=2.8990, c=9.8447, β=48.118

atom	W	x	y	z
Si	2a	0.4153	0	0.0244
Si	2a	0.2896	0	0.8078
Si	2a	0.9895	0	0.2421
C	2a	0.0330	0	0.0248

O	2a	0.8301	0	0.7025
O	2a	0.4312	0	0.8477
O	2a	0.3849	0	0.3472
O	2a	0.1870	0	0.2006

Si_4CO_6; Spgr.: *R*3 (146), Z=3; a=7.8778, c=7.4437

atom	W	x	y	z
Si	3a	0	0	0.2702
Si	9b	0.4152	0.1337	0.2790
C	3a	0	0	0.0136
O	9b	0.8970	0.2934	0.0610
O	9b	0.2653	0.4430	0.0031

Si_5CO_8; Spgr.: *P*1 (1), Z=1; a=5.1785, b=7.9997, c=5.1101 α=91.715, β=116.641, γ=108.657

atom	W	x	y	z
Si	1a	0.3673	0.0351	0.2748
Si	1a	0.1247	0.6323	0.5006
Si	1a	0.7222	0.7169	0.9657
Si	1a	0.9702	0.9508	0.5970
Si	1a	0.5235	0.4262	0.5358
C	1a	0.0680	0.8395	0.3357
O	1a	0.2580	0.0634	0.9284
O	1a	0.2527	0.5072	0.3707
O	1a	0.7235	0.0442	0.4163
O	1a	0.3759	0.2101	0.4547
O	1a	0.7958	0.4965	0.4523

O	1a	0.3707	0.7117	0.8674
O	1a	0.6758	0.5047	0.8919
O	1a	0.7765	0.7938	0.6993

$Si_7C_1O_{12}$; Spgr.: *P* 1 (1), Z=1; a=9.6175, b=5.1873, c=6.4427, α=101.641, β=76.319, γ=99.278

atom	W	x	y	z
Si	1a	0.1622	0.0473	0.7012
Si	1a	0.6813	0.7420	0.2464
Si	1a	0.1872	0.6242	0.9235
Si	1a	0.9865	0.6650	0.3543
Si	1a	0.8965	0.1115	0.5227
Si	1a	0.6674	0.1644	0.9553
Si	1a	0.4501	0.8907	0.6715
C	1a	0.8467	0.8330	0.3359
O	1a	0.5446	0.7475	0.4580
O	1a	0.9550	0.4025	0.4629
O	1a	0.8163	0.1593	0.7731
O	1a	0.1368	0.6207	0.1765
O	1a	0.1328	0.3404	0.7989
O	1a	0.6516	0.9419	0.0996
O	1a	0.5405	0.1092	0.8179
O	1a	0.0537	0.9571	0.5258
O	1a	0.3572	0.6864	0.8319
O	1a	0.6657	0.4474	0.1049
O	1a	0.3290	0.0252	0.5982
O	1a	0.1080	0.8472	0.8695

$Si_{10}C_1O_{18}$; Spgr.: *P* 1 (1), Z=1; a=9.7683, b=7.0458, c=7.6081, α=117.239, β=70.882, γ=94.950

atom	W	x	y	z
Si	1a	0.8338	0.4698	0.9353
Si	1a	0.4726	0.0573	0.4599
Si	1a	0.8908	0.2933	0.1819
Si	1a	0.5549	0.4614	0.4291
Si	1a	0.5273	0.3728	0.0026
Si	1a	0.3349	0.7555	0.1067
Si	1a	0.0193	0.7343	0.4061
Si	1a	0.4321	0.9131	0.7786
Si	1a	0.8059	0.9129	0.2955
Si	1a	0.9681	0.8194	0.8561
C	1a	0.9159	0.0135	0.1141
O	1a	0.9833	0.4825	0.3133
O	1a	0.6422	0.0276	0.4387
O	1a	0.5023	0.4708	0.2509
O	1a	0.5034	0.1199	0.9164
O	1a	0.7214	0.3665	0.3306
O	1a	0.3175	0.8392	0.9448
O	1a	0.8921	0.8963	0.4419
O	1a	0.0385	0.8292	0.6387
O	1a	0.4161	0.5137	0.9800
O	1a	0.7704	0.6676	0.1646
O	1a	0.5446	0.7027	0.6158
O	1a	0.3712	0.9913	0.6424

O	1a	0.9450	0.5664	0.7873
O	1a	0.6938	0.3802	0.8615
O	1a	0.4317	0.9126	0.2475
O	1a	0.1724	0.7543	0.2517
O	1a	0.4488	0.3085	0.5167
O	1a	0.9200	0.3001	0.9571

USPEX crystal structures description (Table 3.2)

$Si_7C_1O_{12}$; Spgr.: *P* 1 (1), Z=1; a=9.6985, b=5.1546, c=5.1771, α=86.872, β=97.686, γ=92.520

atom	W	x	y	z
Si	1a	0.8309	0.6939	0.2535
Si	1a	0.5794	0.0080	0.4717
Si	1a	0.6770	0.4973	0.7326
Si	1a	0.5243	0.5130	0.1717
Si	1a	0.0498	0.0283	0.0432
Si	1a	0.2974	0.7727	0.4065
Si	1a	0.0639	0.5534	0.6946
C	1a	0.6622	0.6959	0.4070
O	1a	0.8026	0.5598	0.9676
O	1a	0.9115	0.9742	0.1940
O	1a	0.5397	0.5706	0.8641
O	1a	0.5499	0.2009	0.2102
O	1a	0.6762	0.1839	0.6862
O	1a	0.9390	0.5132	0.4519
O	1a	0.1884	0.9729	0.2477
O	1a	0.4236	0.9479	0.5589
O	1a	0.3690	0.5935	0.2131

O	1a	0.0608	0.3205	0.9164
O	1a	0.0415	0.8317	0.8088
O	1a	0.2154	0.5724	0.5913

$Si_5C_1O_8$; Spgr.: *P* 1 (1), Z=1; a=5.2267, b=5.0487, c=7.2209, α=75.191, β=105.705, γ=96.064

atom	W	x	y	z
Si	1a	0.2997	0.0916	0.9597
Si	1a	0.2179	0.7029	0.6979
Si	1a	0.8682	0.1436	0.1724
Si	1a	0.4609	0.0974	0.4015
Si	1a	0.1385	0.6101	0.3070
C	1a	0.1909	0.9832	0.1986
O	1a	0.2770	0.4221	0.8696
O	1a	0.1260	0.9171	0.8021
O	1a	0.6226	0.0503	0.0034
O	1a	0.7547	0.0765	0.3715
O	1a	0.4001	0.4144	0.3919
O	1a	0.9272	0.4770	0.1386
O	1a	0.0283	0.6046	0.5031
O	1a	0.4630	0.8797	0.6132

$Si_6C_1O_{10}$; Spgr.: *P* 1 (1), Z=1; a=6.8714, b=7.1341, c=5.3060, α=109.605, β=45.037, γ=96.867

atom	W	x	y	z
Si	1a	0.5675	0.6172	0.9245
Si	1a	0.5785	0.1822	0.7165

Si	1a	0.7368	0.7739	0.4547
Si	1a	0.3021	0.1324	0.2833
Si	1a	0.1412	0.6698	0.1152
Si	1a	0.9864	0.4808	0.5624
C	1a	0.9433	0.6244	0.3760
O	1a	0.4267	0.1691	0.5223
O	1a	0.7128	0.4084	0.7495
O	1a	0.7518	0.0209	0.5834
O	1a	0.5569	0.7138	0.6938
O	1a	0.0733	0.6052	0.8248
O	1a	0.4600	0.1817	0.0221
O	1a	0.1092	0.2764	0.4048
O	1a	0.2205	0.9052	0.1812
O	1a	0.6615	0.7554	0.1741
O	1a	0.3446	0.5413	0.0475

a,b,c are given in {Å}

W-Wyckoff positions

REFERENCES

[1] P. Colombo, G. Mera, R. Riedel, G.D. Soraru, J. Am. Ceram. Soc., 93 (2010) 1805-1837.

[2] C.G. Pantano, A.K. Singh, H.X. Zhang, J. Sol-Gel Sci. Technol., 14 (1999) 7-25.

[3] T. Rouxel, G.D. Soraru, J. Vicens, J. Am. Ceram. Soc., 84 (2001) 1052-1058.

[4] P. Colombo, R. Riedel, G.D. Soraru, H.-J. Kleebe, Polymer Derived Ceramics: From Nano-Structure to Applications, in, DEStech Publications, Inc., Lancaster, 2010, pp. 130-155.

[5] P. Colombo, R. Riedel, G.D. Soraru, H.-J. Kleebe, Polymer Derived Ceramics: From Nano-Structure to Applications, in, DEStech Publications, Inc., Lancaster, (2010) 469.

[6] E. Ionescu, H.J. Kleebe, R. Riedel, Chem. Soc. Rev., 41 (2012) 5032-5052.

[7] H.J. Kleebe, C. Turquat, G.D. Soraru, J. Am. Ceram. Soc., 84 (2001) 1073-1080.

[8] R.J.P. Corriu, D. Leclercq, P.H. Mutin, A. Vioux, J. Mat. Sci., 30 (1995) 2313-2318.

[9] A. Saha, R. Raj, J. Am. Ceram. Soc., 90 (2007) 578-583.

[10] F.M. Wahl, R.E. Grim, R.B. Graf, Am. Mineral., 46 (1961) 196-208.

[11] H.J. Kleebe, G. Gregori, F. Babonneau, Y.D. Blum, D.B. MacQueen, S. Masse, Int. J. Mater. Res., 97 (2006) 699-709.

[12] S. Martinez-Crespiera, E. Ionescu, H.J. Kleebe, R. Riedel, J. Eur. Ceram. Soc., 31 (2011) 913-919.

[13] R.M. Morcos, A. Navrotsky, T. Varga, Y. Blum, D. Ahn, F. Poli, K. Muller, R. Raj, J. Am. Ceram. Soc., 91 (2008) 2969-2974.

[14] P. Kroll, J. Mater. Chem., 20 (2010) 10528-10534.

[15] P. Kroll, J. Mater. Chem., 13 (2003) 1657-1668.

[16] P. Kroll, J. Non-Cryst. Solids, 351 (2005) 1121-1126.

[17] P. Hohenberg, W. Kohn, Phys. Rev. B, 136 (1964) 864-871.

[18] D.M. Teter, R.J. Hemley, G. Kresse, J. Hafner, Phys. Rev. Lett., 80 (1998) 2145-2148.

[19] P. Kackell, B. Wenzien, F. Bechstedt, Phys. Rev. B, 50 (1994) 10761-10768.

[20] H. Brequel, J. Parmentier, S. Walter, R. Badheka, G. Trimmel, S. Masse, J. Latournerie, P. Dempsey, C. Turquat, A. Desmartin-Chomel, L. Le Neindre-Prum, U.A. Jayasooriya, D.

Hourlier, H.J. Kleebe, G.D. Soraru, S. Enzo, F. Babonneau, Chem. Mater., 16 (2004) 2585-2598.

[21] A. Saha, R. Raj, D.L. Williamson, J. Am. Ceram. Soc., 89 (2006) 2188-2195.

[22] T. Varga, A. Navrotsky, J.L. Moats, R.M. Morcos, F. Poli, K. Muller, A. Sahay, R. Raj, J. Am. Ceram. Soc., 90 (2007) 3213-3219.

[23] C.J. Pickard, R.J. Needs, J. Phys. Condens. Matter., 23 (2011) 053201.

[24] G. Kresse, J. Hafner, Phys. Rev. B, 47 (1993).

[25] G. Kresse, J. Hafner, Phys. Rev. B, 49 (1994) 14251-14269.

[26] G. Kresse, J. Furthmuller, Comp. Mater. Sci., 6 (1996) 15-50.

[27] J.F. G. Kresse, Phys. Rev. B, 54 (1996).

[28] C.W. Glass, A.R. Oganov, N. Hansen, Comput. Phys. Commun., 175 (2006) 713-720.

[29] G.L. Weerasinghe, R.J. Needs, C.J. Pickard, Phys. Rev. B, 84 (2011).

[30] S.J. Widgeon, S. Sen, G. Mera, E. Ionescu, R. Riedel, A. Navrotsky, Chem. Mater., 22 (2010) 6221-6228.

[31] B. Homez, H.-J. Michel, J. Halbritter, J. Mater. Res., 9 (1994) 7.

[32] H.A. Hoppe, F. Stadler, O. Oeckler, W. Schnick, Angew. Chem. Int. Edit., 43 (2004) 5540-5542.

[33] V. Bachmann, C. Ronda, O. Oeckler, W. Schnick, A. Meijerink, Chem. Mater., 21 (2009) 316-325.

[34] M. Hillert, S. Jonsson, Z. Metallkd., 83 (1992) 720-728.

[35] P. Kroll, M. Milko, Z. Anorg. Allg. Chem., 629 (2002) 1737-1750.

[36] L. Bois, J. Maquet, F. Babonneau, H. Mutin, D. Bahloul, Chem. Mater., 6 (1994) 796-802.

[37] G.D. Soraru, G. Dandrea, R. Campostrini, F. Babonneau, G. Mariotto, J. Am. Ceram. Soc., 78 (1995) 379-387.

[38] C. Turquat, H.J. Kleebe, G. Gregori, S. Walter, G.D. Soraru, J. Am. Ceram. Soc., 84 (2001) 2189-2196.

[39] G.M. Renlund, S. Prochazka, R.H. Doremus, J Mater Res, 6 (1991) 2723-2734.

[40] G. Trimmel, R. Badheka, F. Babonneau, J. Latournerie, P. Dempsey, D. Bahloul-Houlier, J. Parmentier, G.D. Soraru, J. Sol-Gel Sci. Technol., 26 (2003) 279-283.

[41] J. Brus, F. Kolar, V. Machovic, J. Svitilova, J. Non-Cryst. Solids, 289 (2001) 62-74.

[42] Q. Zhu, A.R. Oganov, A.O. Lyakhov, Crystengcomm, 14 (2012) 3596-3601.

[43] Z.G. Bazhanova, A.R. Oganov, O. Gianola, Phys-Usp., 55 (2012) 489-497.

BIOGRAPHICAL INFORMATION

Nelli Bodiford became a full-time student at the University of Texas at Arlington in 2006 and in 2010, where she earned her B.S. degree in biology with the minors in chemistry and German language. As an undergraduate in 2008 she participated in Honors College summer research program, URA (Undergraduate Research Assistantship) and completed a research project under the supervision of professor Peter Kroll. In the following summer of 2009, she was chosen to participate in the REU (Research Experience for Undergraduates) program sponsored by NSF. During that time, she worked on the project with the professor Dr. Thomas Cundari at the University of North Texas. The project was completed successfully and resulted in a publication.

In 2010 Nelli was accepted into a graduate program in chemistry at the University of Texas at Arlington. Within her fist year she made a decision to join a research group led by professor Peter Kroll. Her work is solely in the theoretical-computational field. After three years of working in the lab, Nelli is graduating with her Master's degree in May of 2013. She wants to continue with the graduate studies after she receives her Master's degree. She believes that as a woman her contribution will benefit the school and add to a diverse research group that she wants to join. While her training is concentrated exclusively in computational materials chemistry, she is willing to explore other fields of chemistry research.